JOURNAL OF MAGNETIC RESONANCE **131,** 8–16 (1998)
ARTICLE NO. MN971316

Effects of Sandimmune Neoral on Collagen-Induced Arthritis in DA Rats: Characterization by High Resolution Three-Dimensional Magnetic Resonance Imaging and by Histology

Nicolau Beckmann,* Konrad Bruttel,* Henk Schuurman,† and Anis Mir‡

*Core Technologies,† Transplantation, and ‡Arthritis and Bone Metabolism Areas, Novartis Pharma Inc., CH-4002 Basel, Switzerland

Received May 2, 1997; revised September 30, 1997

In the present work the time course of collagen-induced arthritis and the effect of Sandimmune Neoral in this model of arthritis were followed in the rat over an extended period of time (70 days) using high resolution three-dimensional (3D) magnetic resonance imaging (MRI). High resolution 3D gradient-echo (TR = 100 ms; TE = 3.8 ms) images with a voxel size of 94 × 81 × 60 μm^3 were acquired from the hind paw of DA rats (n = 21) at various time points after injection of type II bovine collagen into the tail. Eleven rats were treated with Neoral (15 mg/kg/day p.o. together with vehicle) for 42 days starting at day 14 after collagen injection. The remaining controls received vehicle. Pathomorphological changes associated with the collagen-induced arthritic process, e.g., increase of joint space and cartilage and bone erosion, could be observed *in vivo* **in the control group. In contrast, no changes in the joint architecture were detected in Neoral-treated animals. Indeed, Neoral showed strong anti-inflammatory effects and marked protection against cartilage and bone destruction in this model. Qualitative information derived from the MR images correlated significantly with histological findings.**

Key Words: **collagen-induced arthritis; high resolution MRI; cartilage; cyclosporine; Sandimmune Neoral.**

INTRODUCTION

Rheumatoid arthritis (RA) is a chronic systemic inflammatory disease characterized by synovial inflammation and progressive destruction of the articular cartilage and tissue (*1*). Major efforts are currently being undertaken to develop novel therapies with ''disease controlling'' properties. A prerequisite for development of such drugs is the use of relevant animal models that mimic the clinical features of the disease (*2*).

Due to its noninvasive character and its ability to distinguish between cartilaginous and bony tissues, MRI is an interesting approach to studying the effects of drugs on the articular structures during the disease process (*3–5*). For instance, it has been shown recently that the arthritic process induced in the rat by immunization with heterologous collagen can be followed noninvasively in the hind paw with high-resolution three-dimensional (3D) MRI techniques (*6*). Using this approach, distinct pathomorphological changes associated with the collagen-induced arthritic process (e.g., increase of joint space, and cartilage and bone erosion) can be analyzed *in vivo* (*6*).

There are several pieces of evidence indicating that T-cells play an important role in the pathogenesis of RA (*7*). Cyclosporine (Sandimmune) is a T-cell inhibitor which has been shown to be effective in the treatment of chronic refractory RA patients (*8*) and also in a number of animal models of rheumatoid arthritis (*9, 10*). Sandimmune Neoral, which is a microemulsion-based formulation, has been shown in the clinic to have better pharmacokinetic and absorption characteristics than Sandimmune (*11*).

In the present work we used high resolution 3D MRI techniques to characterize the effects of Sandimmune Neoral on the progression of heterologous type II collagen-induced arthritis (*12, 13*) in the hind paw of the DA rat. Additionally, histological analysis was performed to validate the results obtained with MRI.

MATERIALS AND METHODS

Animals and treatment regime. Female DA rats were divided into two groups: (i) rats (n = 11, 151 ± 2 g, 10 weeks old at the beginning of the study) treated with Sandimmune Neoral (15 mg/kg/day administered p.o.) for 42 days starting 14 days after immunization with type II bovine collagen, and (ii) controls (n = 10, 153 ± 2 g, 10 weeks old at the beginning of the study) receiving vehicle (Neoral microemulsion) p.o. in a volume of 5 ml/kg. The dose of Neoral was chosen from prior dose–response studies in this model. Only responders to the immunization with collagen were included in the study, i.e., only animals already showing significant paw swelling on day 14 after collagen injection (72% of the immunized rats).

Immunization process. Bovine nasal septum type II collagen (Elastin Products Co., Owensville, Missouri) was dissolved in 0.1 M acetic acid at 4°C and this collagen solution was emulsified with an equal volume of Freund's incomplete

1090-7807/98 $25.00

adjuvant (DIFCO Laboratories, Michigan, USA). All rats were immunized intradermally around the base of the tail at multiple sites with 400 μl (0.6 mg/rat) of the emulsion. An analgesic, Temgesic (Reckit & Colman, Hull, England; 0.015 mg/animal), was administered subcutaneously 20 min prior to immunization.

MR methods. Measurements were carried out with a Bruker Biospec 47/40 system operating at 4.7 T and equipped with an actively shielded gradient set capable of generating gradient strengths up to 180 mT/m in 100 ms. The operational software of the MR system was UXNMR running on an ASPECT X32 computer. High resolution 3D images were acquired using the gradient-echo technique. A home-built resonator with a sample space of dimensions 13 $\times$ 5 $\times$ 20 mm^3 was used for excitation and detection (*6*). Acquisition parameters were the following: field of view 12 $\times$ 5.2 $\times$ 15.4 mm^3, matrix size 128 $\times$ 64 $\times$ 256, and sweep width 50 kHz. The resulting voxel size of the images was 94 $\times$ 81 $\times$ 60 μm^3. The repetition time was set to 100 ms and the echo time to 3.8 ms. Rectangular excitation pulses of 200 μs duration were applied. Two averages were recorded, resulting in a total measurement time of 54.6 min for each 3D data set.

Animals were imaged at the following time points after immunization: day 14 (11 treated, 10 controls), day 32 (11 treated, 10 controls), day 40 (10 treated, 8 controls), day 55 (8 treated, 8 controls), day 63 (6 treated, 6 controls), and day 70 (4 treated, 4 controls). During the MRI investigations the rats were anaesthetized with 1.5–2% isoflurane (Abbott, Cham, Switzerland) in a mixture of oxygen/nitrous oxide (1:2) administered via a face mask and positioned on an animal support made of plexiglass. The position of the right hind paw within the home-built resonator was verified with two-dimensional scout views [spin–echo sequence (TR = 500 ms/TE = 19 ms), measurement time 1 min] prior to the 3D acquisition.

Assessment of paw swelling and joint gap volume. Swelling was assessed by measuring the external thickness of the hind paws in the region of the metatarsals using a microcaliper. The volumes of the metatarsophalangeal (MTP) and the proximal interphalangeal (ITP) joint gaps of toe III were assessed by an observer unaware of the treatment from the 3D images using the procedure described in detail in (*6*). For each 3D data set, the volume was determined by adding the areas corresponding to the joint gap in slices covering the proximal ITP and the MTP joints, and multiplying by the effective slice thickness. Areas were assessed using standard software from the equipment. In the delineation of the region of interest (ROI) covering the gap of a joint in a typical slice the lateral limits were chosen tangentially to the two bones, while the upper and lower limits of the ROI were provided by the bones themselves. The ROI was redefined for each individual slice.

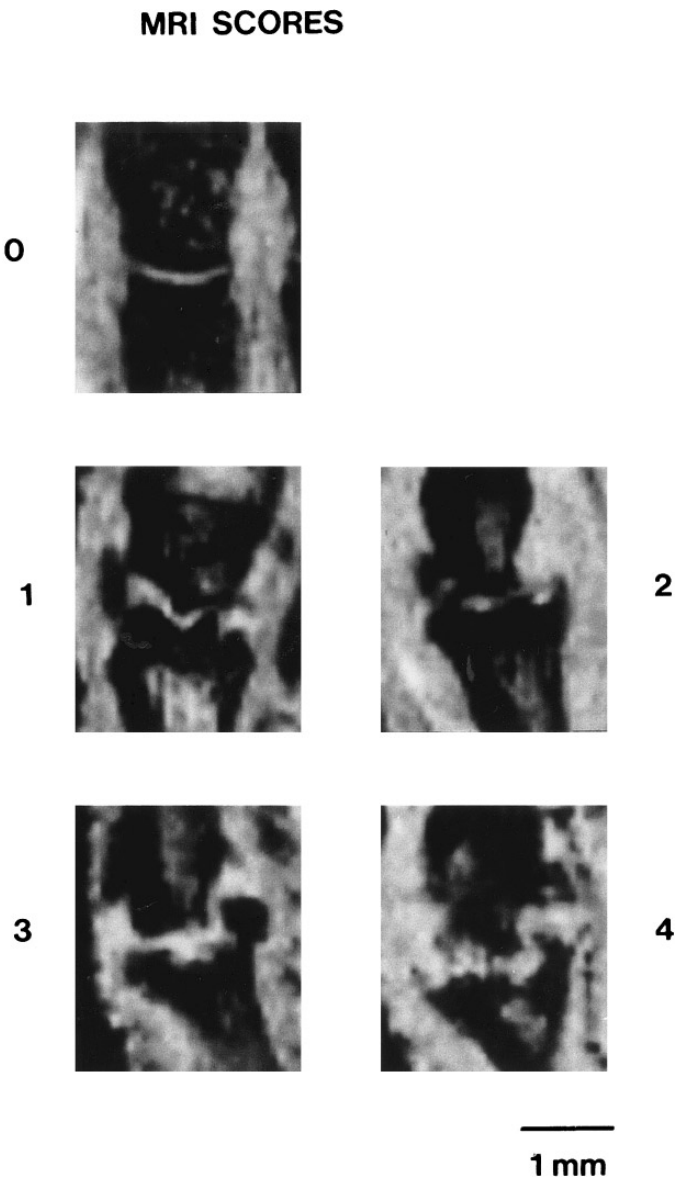

FIG. 1. MRI scores, described in Materials and Methods.

MRI scores. Joints displayed on MR images (Fig. 1) were scored as follows: 0, normal joint; 1, normal bone structure, but an increase of the joint space can be noticed; 2, slight bone erosion on one side of the joint; 3, extensive bone erosion on one side, and slight bone erosion on the other side of the joint; 4, extensive bone erosion on both sides of the joint, with loss of the joint architecture. The score given to each joint is an average for several slices of the 3D MRI data set covering the joint.

Histology procedures. At autopsy, the whole right hind paw was removed and fixed in phosphate-buffered formalin. After decalcification and embedding in paraffin, three sections were prepared along the sagittal direction from

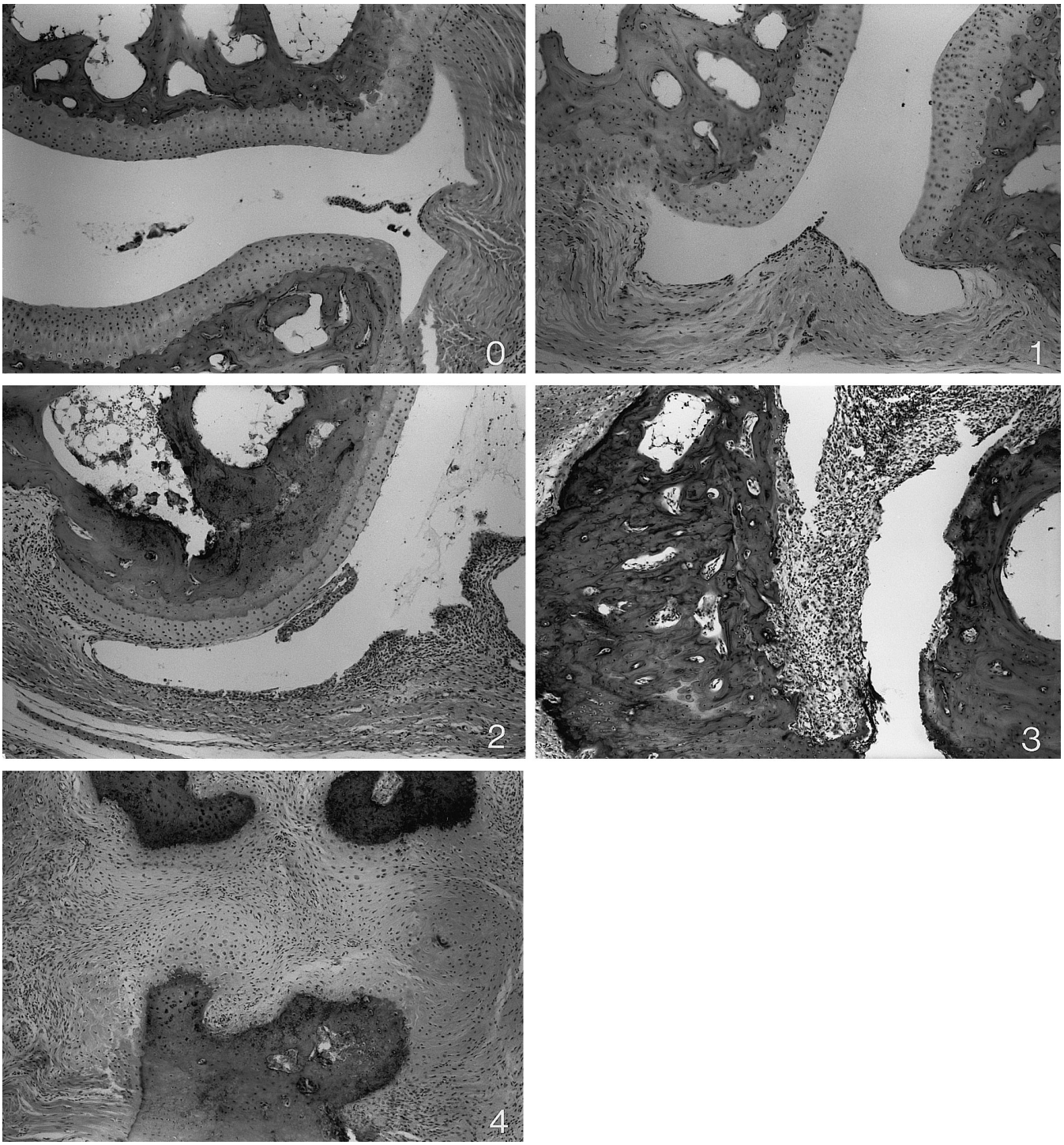

FIG. 2. Histology scores, described in Materials and Methods.

each selected joint. In case more joints per toe or paw were investigated, this sectioning at three levels was done for the whole toe or paw. Sections were stained with hematoxylin and eosin. Autopsy was performed on the same day as the last MR measurement at various time points during the study to allow a comparison between MRI and histology at different stages of the progression of the arthritic process. The time points for sacrificing the animals

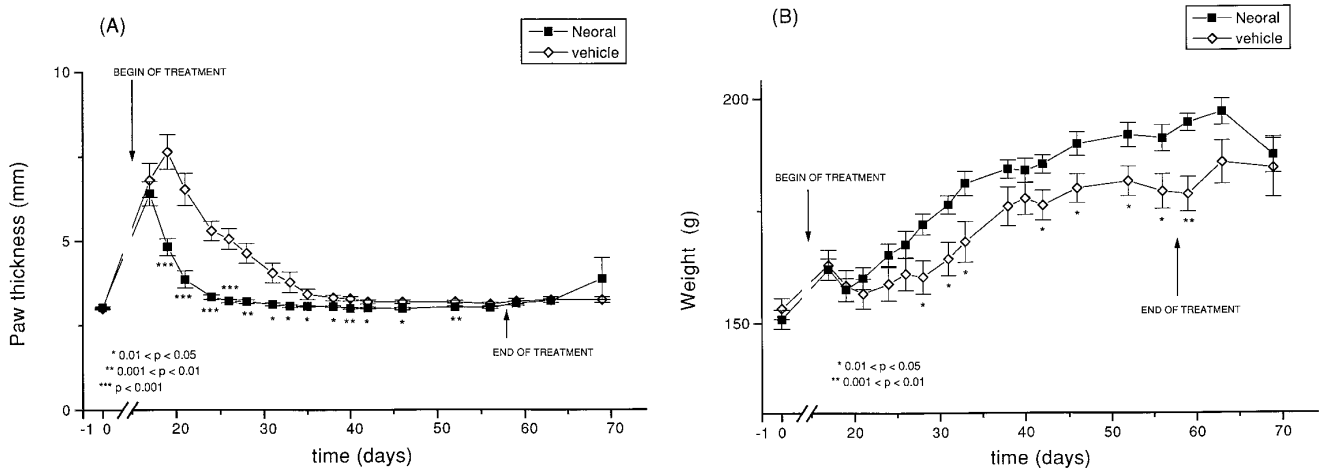

FIG. 3. Development of paw swelling (A) and of the rats' weight (B) during the study.

were chosen based on a previous study concerning the same model, where we showed that a significant increase of the interphalangeal joint space could already be observed at day 30 following collagen administration (*6*). Animals were killed immediately after the MR measurement on day 32 (1 treated, 2 controls), 40 (2 treated), 55 (2 treated, 2 controls), 63 (2 treated, 2 controls), and 70 (4 treated, 4 controls) after immunization.

Histology scores. The relevant joint was identified in each of the three sections. The presence of subsynovial inflammation, destruction of articular cartilage, and general destruction of the joint with pannus formation and bone erosion were scored on a scale 0–4 (Fig. 2): 0, no abnormalities, normal joint feature; 1, marginal destruction of cartilage only and slight inflammation in the articular tissue; 2, extensive inflammation and moderate cartilage destruction with slight bone erosion, usually on one side of the joint only; 3, extensive inflammation and significant destruction of both cartilage and bone; 4, almost complete cartilage destruction, with no intact cartilage left; almost complete loss of the general joint architecture with extensive pannus formation and bone erosion; extensive inflammation in the articular tissue, mainly by mononuclear cells (lymphocytes, plasma cells, macrophages) often accompanied by polymorphonuclear granulocytes. The score given to each joint is an average for the three histological sections through that joint.

Statistical analysis. The nonparametric Spearman rank coefficient of correlation (r_s), corrected for ties, was calculated for the histology and MRI scores. A Student's t-test with independent samples and separate variances was used for the evaluation of significance of effects on paw swelling and joint volumes. A Mann–Whitney nonparametric test was applied to verify if the MRI scores from the treated and the control animals differed significantly.

RESULTS

Effect of Sandimmune Neoral on paw inflammation. Swelling of the paw peaked around 20 days after immunization with collagen in the vehicle-treated animals (controls) and gradually receded over the next 30 days to baseline (Fig. 3A). Neoral treatment was started 14 days after immunization, when significant inflammation had already developed, and continued until day 56. Treatment resulted in a marked and complete inhibition of swelling and the animals gained significantly more weight compared to the control group during the treatment period (Figs. 3A, 3B). After treatment was stopped both groups attained a similar weight within 10 days.

Effect of Sandimmune Neoral on joint architecture. Figure 4 presents MR images with a slice thickness of 81 μm extracted from 3D data sets acquired from two animals at several time points after immunization. Images in Fig. 4 (left) correspond to a control animal, while images in Fig. 4 (right) are from a Neoral-treated rat. The contrast/noise ratio between bone marrow in the metatarsal bone and surrounding muscle tissue was on the order of 14. Note the good anatomical definition of the joints, a consequence of the high spatial resolution attained (voxel size $94 \times 81 \times 60$ μm $= 4.6 \times 10^5$ μm^3). Furthermore, partial volume artefacts were minimal because of the small slice thickness (81 μm). For the control animal, the joint gap had grown considerably between 26 and 40 days after immunization due to the growth of the synovium and the partial erosion of cartilage, as revealed by an edge-sensitive filter (procedure described in Ref. *6*). At a later stage, around 60 days after immunization, the cartilage and the bone itself were severely eroded by the arthritic process, as already described previously (*6*). In contrast, the joint structure of the Neoral-treated rat remained intact (Fig. 4, right).

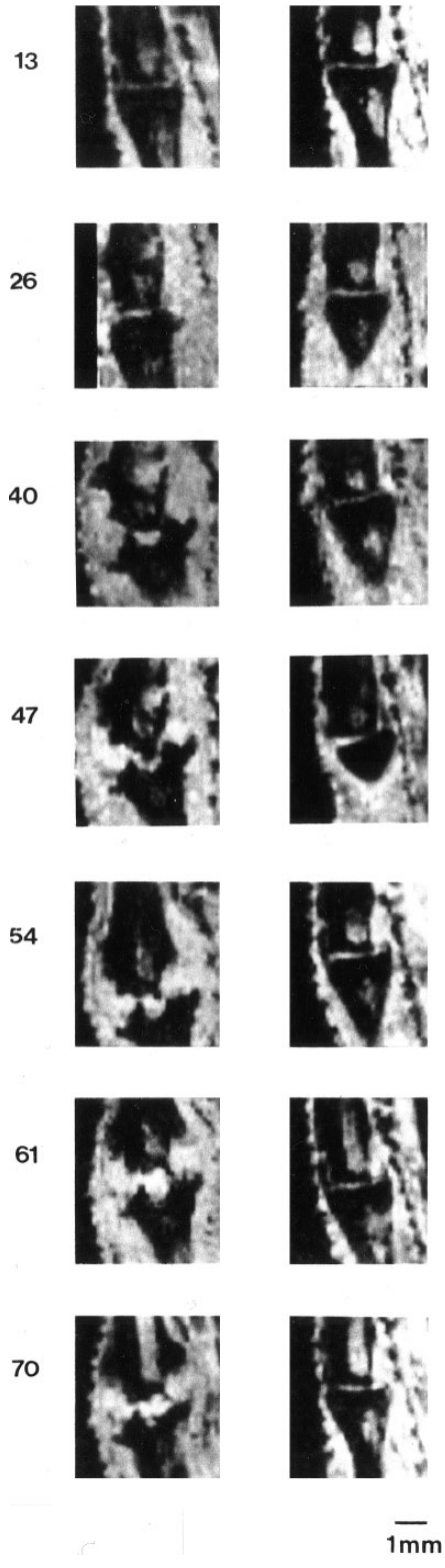

FIG. 4. Time course of the proximal ITP joint architecture for a control (left) and a Neoral-treated rat (right). Images (effective slice thickness: 81 μm; in-plane resolution: 94 $\times$ 60 μm^2) were extracted from 3D data sets acquired at the time points (in days relative to the immunization with type II bovine collagen) specified on the left side of the figure.

The development of the MTP and the proximal ITP joint gap volumes of toe III is presented in Fig. 5. A gradual and dramatic increase of the joint gap volume began to occur about a month after immunization for the control rats. At this stage the external gross swelling of the metatarsal region of the paw had receded (see Fig. 3A). The change in ITP joint volume was more severe ($>$300% increase) than that of the MTP joints (40% increase). The increase in gap volume of both joints was completetely inhibited by Neoral.

The MRI and histology scores of different toes also showed this progressive and marked destruction of the joints in the control group and the protective effect of the Neoral treatment (Fig. 6). For the control group, a marked destruction of ITP joints was observed (about 80% of proximal ITP joints scored $\geq$3), while MTP joints were affected less severely (about 76% of joints scored $\leq$1). In contrast, all MTP joints and more than 84% of proximal ITP joints of Neoral-treated rats received scores $\leq$1. The nonparametric Spearman rank coefficient of correlation between the MRI and the histology scores, corrected for ties, was of 0.93 for the controls ($p < 0.01$). The time courses of the MRI scores for toe I are illustrated in Fig. 7.

DISCUSSION

A prerequisite for drug development is the establishment of relevant animal models that mimic the pathological process occurring in humans. The model of arthritis used in this work features several characteristics of the human disease (*2, 12, 13*). Analysis of the morphological changes constitutes an important aspect of model characterization. Because of the progressive nature of the disease process, it is essential to monitor changes in the skeletal structures over time. Ideally, the effects of the disease process on the skeletal structures should be followed noninvasively with good spatial resolution and repetitive measurements performed on the same animal. The voxel size of the paw images, 94 $\times$ 81 $\times$ 60 μm^3, was enough to characterize the progression of the collagen-induced arthritic process in the rat paw *in vivo.* A key factor in the quality of the images was the use of an optimized radiofrequency probe. The resonator had a very homogeneous radiofrequency distribution, which was particularly advantageous for 3D acquisitions. Additionally, it simplified the positioning of the paw.

It has been reported previously that the administration of contrast agents (*3, 14*) or the application of saturation transfer and fat-suppressed T_1-weighted sequences (*4, 5*) could improve the characterization of the cartilage and of the synovium in the interphalangeal joints. In the present study, we avoided the application of contrast agents for practical reasons. Furthermore, fat suppression did not significantly improve the characterization of cartilage in the paw joints.

We consider the 3D imaging modality essential for the kind of applications envisaged here because of (i) easy posi-

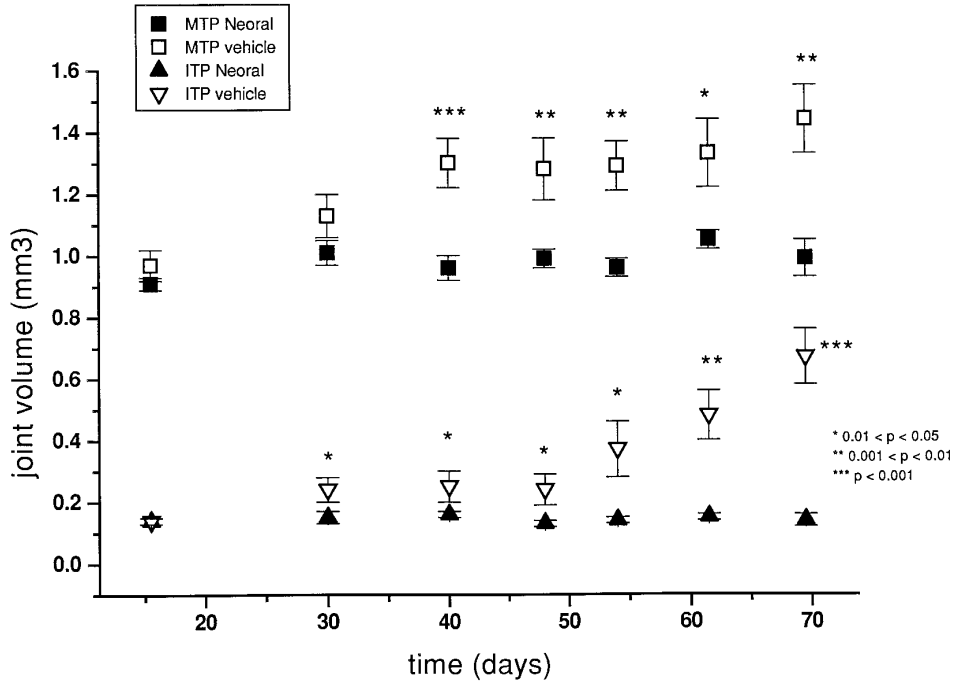

FIG. 5. Development of the joint gap volume of MTP and proximal ITP joints of toe III after immunization with 0.6 mg/rat type II bovine collagen for control and Neoral-treated rats.

tioning of imaging slices by postprocessing and (ii) less pronounced partial volume effects than in corresponding high-resolution 2D images (*15*) due to the significant smaller slice thickness (81 vs 400 μm). These properties of 3D imaging improve the interpretation and comparison of images acquired in different measurement sessions. Furthermore, the total duration of a 3D examination, about 1 h, is acceptable when examining a larger number of animals. The additional possibility of deriving quantitative information from the 3D data sets, e.g., assessment of the volume of the joint gap as shown in Fig. 5, also allows better characterization of the arthritic process in the course of drug testing.

MR images of the immunized and untreated rats showed distinct pathomorphological changes in the joint structures. Compared to the images acquired prior to immunization, the joint gap began to increase significantly between 26 and 40 days after immunization (Figs. 4 and 5). Furthermore, a partial disruption of cartilage could already be observed in some of the joints at these time points by applying an edge-sensitive filter to the acquired images as described in (*6*). Around 60 days after immunization the images revealed severe destruction of cartilage and erosion of bony structures (Fig. 4). The anatomical changes observed by MRI in the proximal ITP and MTP joints were preceded by gross swelling of the paws in the metatarsal region, which peaked around day 20 after immunization, in accordance with results from the literature (*12*). MRI is therefore an important tool in following the chronic joint-destructive stage of the disease. Interesting to note is the fact that the ITP joints were affected more severely and earlier by the arthritic process than the MTP joints (see Figs. 5–7).

Sandimmune Neoral showed a strong anti-inflammatory effect (Fig. 3A) and a clear joint protective effect (Figs. 4 and 5) in the present study. There was no increase in volume of the joint gaps in Neoral-treated animals, in contrast to the control group, where the increase in joint gap volume was substantial (Fig. 5). In addition, all the MTP joints and 84% of the proximal ITP joints analyzed for animals in the Neoral-treated group received low scores ($\leq$1). In contrast, for the control group 76% of the MTP joints and only 16% of the proximal ITP joints received low scores ($\leq$1), while 80% of the proximal ITP joints received high scores ($\geq$3). Qualitative information derived from the MR data sets correlated significantly with the histologic findings (nonparametric Spearman rank coefficient of correlation, corrected for ties, of 0.93, $p < 0.01$, for controls).

The effectiveness of cyclosporine in experimental models of joint inflammation and articular damage has been documented (*9, 10, 16*). It is also effective in disease modification of chronic refractory RA patients (*8*). Thus, the results obtained in the present study confirm and extend the previously reported effects of cyclosporine in animal models of arthritis since (i) data collection occurred *in vivo* and (ii) a microemulsion-based formulation of cyclosporine was

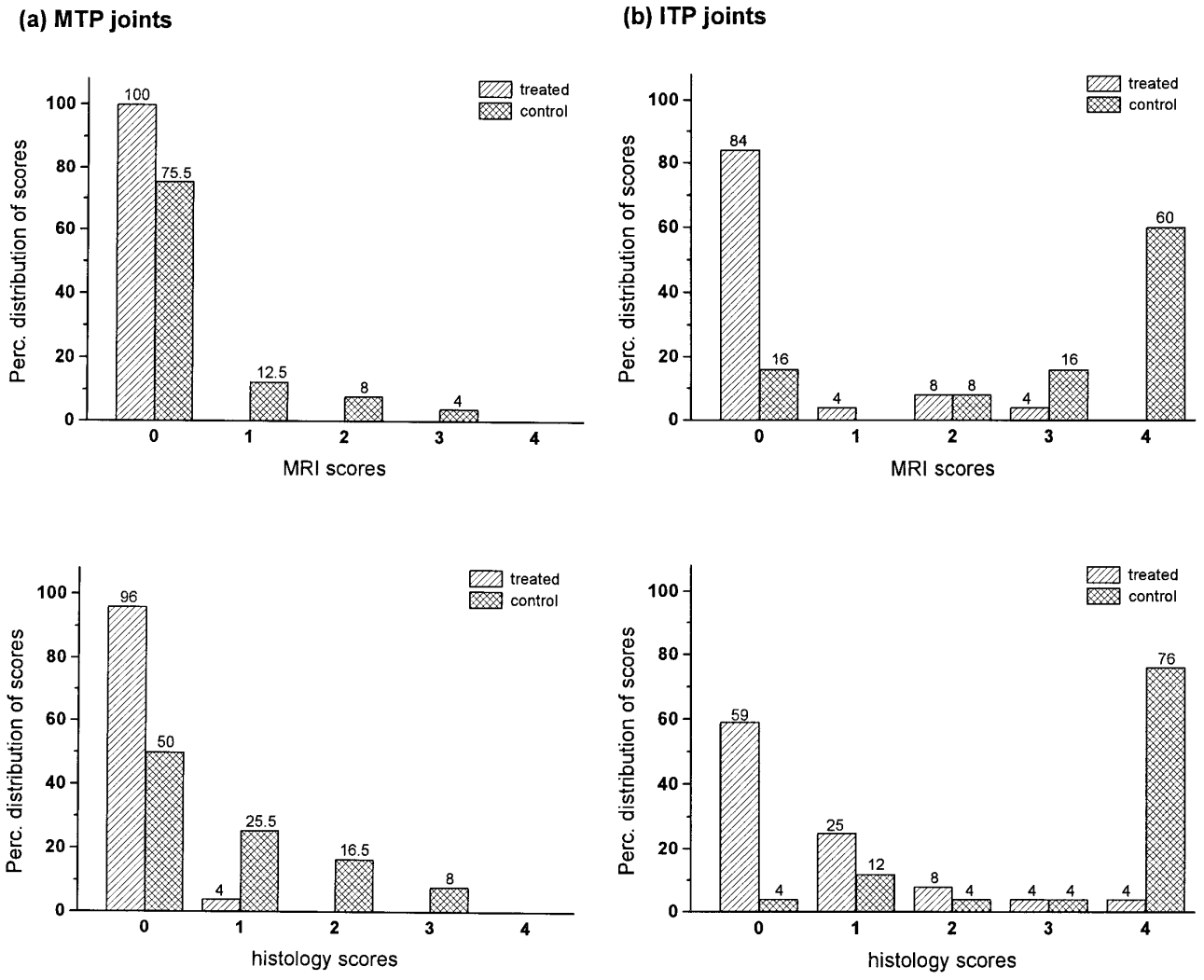

FIG. 6. Percentual distribution of the MRI and histology scores assigned to (a) MTP joints and (b) ITP joints of Neoral-treated rats (24 joints, 11 animals) and of control rats (24 joints, 10 animals). Percentile values are indicated above the respective bars.

tested. As regards its mechanism of action cyclosporine is a potent immunomodulatory agent and its major action is inhibition of the production of cytokines involved in T-cell activation (*17*). There is also evidence for direct or indirect effects of cyclosporine on other cells of the immune system and bone and connective tissue (*18*) that, together with T cells, play an important role in the articular joint destruction in animal models of arthritis and in RA.

There is some controversy in the literature concerning the degree of osteopenia after treating normal rats with cyclosporine. Administration of 15 mg/kg of cyclosporine for a 4-week period has been reported to produce an average reduction of 57% in tibial trabecular volume (*19*). Other studies have shown that such an effect could only be produced by administering toxic doses of the compound. Bertolini *et al.* have reported that treatment of young growing rats with 25 mg/kg cyclosporine decreased trabecular and cortical bone thickness by only 13% and 21% ($p < 0.02$), respectively (*20*). These results agree with a study by del Pozo *et al.* (*21*), who found that in female Wistar rats, 7 weeks of age and average weight of 176 g receiving daily 15 mg/kg cyclosporine orally for 30 days, total skeletal mineral content was not modified, whereas tibial trabecular volume was lowered by only 16.3% ($p < 0.02$). However, no report is available concerning trabecular losses in the joints of the paw of the rat. The resolution of the images in the present study is not sufficient to allow a quantification of the trabecular structure.

Another useful technique for osteoarthritis studies on animals, especially on the chronic phase, is peripheral Quantitative Computed Tomography (pQCT) (*22*). This technique is applied routinely in preclinical studies to monitor changes

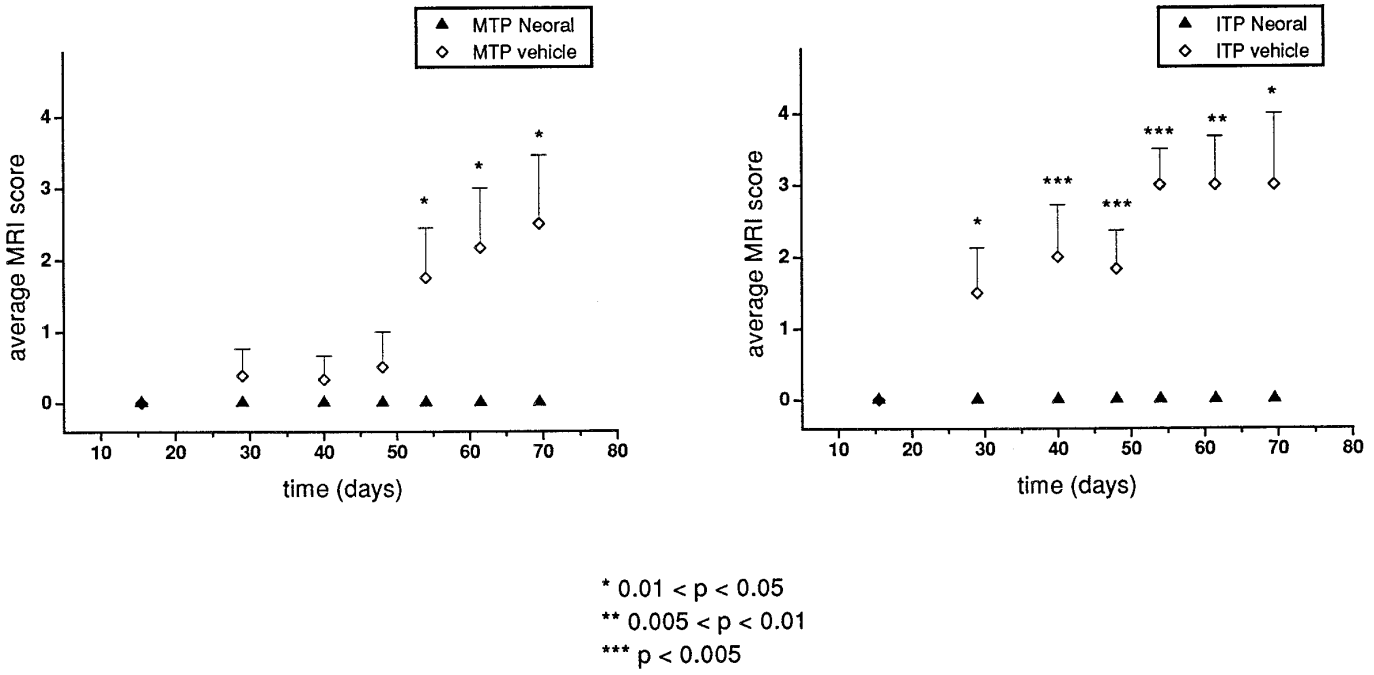

FIG. 7. Time course of the average scores for the MTP and proximal ITP joints of toe I, derived from MR images acquired at several time points during the study.

in bone mass and density of the rat tibia. However, it provides a resolution of only 0.2×0.2 mm^2 *in vivo* at a slice thickness of 1 mm, thus being of limited use for the present application on the paw of the rat. A further limitation of pQCT is the fact that soft-tissue changes, like synovial enhancement and edema formation, as well as cartilage losses, cannot be followed.

REFERENCES

1. N. O. Rottermich and R. L. Whisler, ''Rheumatoid Arthritis,'' Grune & Stratton, San Diego (1985).
2. L. Klareskog, What can we learn about rheumatoid arthritis from animal models?, *Springer Sem. Immunopathol.* **11,** 315–333 (1989).
3. J. C. Waterton, V. Rajanayagam, B. D. Ross, D. Brown, A. Whittemore, and D. Johnstone, Magnetic resonance methods for measurement of disease progression in rheumatoid arthritis, *Magn. Reson. Imaging* **11,** 1033–1038 (1993).
4. C. G. Peterfy, S. Majumdar, P. Lang, C. F. van Dijke, K. Sack, and H. K. Genant, MR imaging of the arthritic knee: Improved discrimination of cartilage, synovium, and effusion with pulsed saturation transfer and fat-suppressed T_1-weighted sequences, *Radiology* **191,** 413–419 (1994).
5. M. P. Recht, D. W. Piraino, G. A. Paletta, J. P. Schils, and G. H. Belhobek, Accuracy of fat-suppressed three-dimensional spoiled gradient-echo FLASH MR imaging in the detection of patellofemoral articular cartilage abnormalities, *Radiology* **198,** 209–212 (1996).
6. N. Beckmann, K. Bruttel, A. Mir, and M. Rudin, Noninvasive 3D MR microscopy as a tool in pharmacological research: Application to a model of rheumatoid arthritis, *Magn. Reson. Imaging* **13,** 1013–1017 (1995).
7. G. Panayi, J. S. Lanchbury, and G. H. Kingsley, The importance of the T cell in initiating and maintaining the chronic synovitis of rheumatoid arthritis, *Arthritis Rheum.* **35,** 729–735 (1992).
8. C. Richardson and P. Emery, Clinical use of cyclosporine in rheumatoid arthritis, *Drugs* **50** (Suppl. 1), 26–36 (1996).
9. R. L. Wong, Mechanisms of action of cyclosporine A in animal models of rheumatoid arthritis, *Inflammopharmacology* **2,** 177–195 (1993).
10. E. Del Pozo, M. Graeber, P. Elford, and T. Payne, Regression of bone and cartilage loss in adjuvant arthritic rats after treatment with cyclosporine A, *Arthritis Rheum.* **33,** 247–252 (1990).
11. S. Noble and A. Markham, Cyclosporine: a review of the pharmacokinetic properties, immunosuppressive efficacy and tolerability of a microemulsion-based formulation (Neoral), *Drugs* **50,** 924–941 (1995).
12. D. E. Trentham, A. S. Townes, and A. H. Kang, Autoimmunity to type II collagen: An experimental model of arthritis, *J. Exp. Med.* **77,** 857–868 (1977).
13. R. Holmdahl, L. Jansson, D. Gullberg, P. O. Forsberg, K. Rubin, and L. Klareskog, Incidence of arthritis and auto-reactivity of anti-collagen antibodies after immunization of heterologous and autologous collagen II, *Clin. Exp. Immunol.* **62,** 639–646 (1985).
14. C. M. P. Hervé-Somma, G. H. Sebag, A.-M. Prieur, V. Bonnerot, and D. P. Lallemand, Juvenile rheumatoid arthritis of the knee: MR evaluation with Gd-DOTA, *Radiology* **182,** 93–98 (1992).
15. N. Beckmann, M. Rudin, and A. Mir, MR microscopy of the rat interphalangeal joints *in vivo:* Application to a model of rheumatoid

arthritis, *in* ''Proceedings, SMRM, 12th Annual Meeting, New York, 1993,'' p. 939.

16. G. W. Cannon, S. McCall, B. C. Cole, L. A. Radov, J. R. Ward, and M. M. Griffiths, Effects of gold sodium thiomolate, cyclosporin A, cyclophosphamide, and placebo on collagen-induced arthritis in rats, *Agents Actions* **38,** 240–246 (1993).

17. F. E. Di Padova, Pharmacology of cyclosporine (Sandimmune). V. Pharmacological effects on immune function: *In vitro* studies, *Pharmacol. Rev.* **41,** 373–406 (1989).

18. G. Russell, R. Graveley, J. Seid, A. K. al-Humidan, and H. Skodt, Mechanisms of action of cyclosporine and effects on connective tissue, *Semin. Arthritis Rheum.* **21** (6, Suppl. 3), 16–22 (1992).

19. C. Movsowitz, C. Epstein, M. Fallon, F. Ismail, and S. Thomas, Cyclosporine-A *in vivo* produces severe osteopenia in the rat: Effect of dose and duration of administration, *Endocrinology* **123,** 2571–2577 (1988).

20. D. R. Bertolini, A. Badger, and W. High, Effect of immunomodulators on bone in the rapidly growing rat, *J. Bone Miner. Res.* **8** (Suppl. 1), 315 (1993).

21. E. del Pozo, K. Lippuner, W. Ruch, J. P. Casez, T. Payne, A. MacKenzie, and P. Jaeger, Different effects of Cyclosporine A on bone remodeling in young and adult rats, *Bone* **16** (4, Supplement), 217S–275S (1995).

22. J. A. Gasser, Assessing bone quantity by pQCT, *Bone* **17** (4, Supplement), 145S–154S (1995).